View metadata, citation and similar papers at core.ac.uk

brought to you by CORE

provided by Radboud Repository

Radboud Repository

Radboud University Nijmegen

PDF hosted at the Radboud Repository of the Radboud University Nijmegen

The following full text is a publisher's version.

For additional information about this publication click this link.
http://hdl.handle.net/2066/92231

Please be advised that this information was generated on 2017-12-06 and may be subject to change.

View Online / Journal Homepage / Table of Contents for this issue

Product pair correlation in CH_3OH photodissociation at 157 nm: the OH + CH_3 channel

Zhichao Chen,[ab] Andre T. J. B. Eppink,[b] Bo Jiang,[a] Gerrit C. Groenenboom,[c] Xueming Yang*[a] and David H. Parker*[b]

Received 13th September 2010, Accepted 29th October 2010
DOI: 10.1039/c0cp01794a

Published on 26 November 2010 on http://pubs.rsc.org | doi:10.1039/C0CP01794A
Downloaded by Radboud Universiteit Nijmegen on 06 November 2012

The OH + CH_3 product channel for the photodissociation of CH_3OH at 157 nm was investigated using the velocity map imaging technique with the detection of CH_3 radical products *via* (2+1) resonance-enhanced multiphoton ionization (REMPI). Images were measured for the CH_3 formed in the ground and excited states (v_2 = 0, 1, 2, and 3) of the umbrella vibrational mode and correlated OH vibrational state distributions were also determined. We find that the vibrational distribution of the OH fragment in the OH + CH_3 channel is clearly inverted. Anisotropic distributions for the CH_3 (v_2 = 0, 1, 2, and 3) products were also determined, which is indicative of a fast dissociation process for the C–O bond cleavage. A slower CH_3 product channel was also observed, that is assigned to a two-step photodissociation process, in which the first step is the production of a $CH_3O(X\ ^2E)$ radical *via* the cleavage of the O–H bond in CH_3OH, followed by probe laser photodissociation of the nascent CH_3O radicals yielding $CH_3(X\ ^2A_1, v = 0)$ products.

1. Introduction

Methanol, the smallest alcohol, is an important species in both the atmospheres of Earth[1] and comets,[2–4] and in interstellar media.[5] The photochemistry of CH_3OH has received considerable attention over the last two decades.[6,7] Vacuum ultraviolet (VUV) photolysis of methanol is also a challenging and interesting problem where multiple dissociation pathways on multiple electronic surfaces are likely. In addition, the relatively small number of electrons in methanol makes it amenable to high-level computational studies.

Numerous studies on the absorption spectra[8–10] of methanol have been carried out. Nee *et al.*[8] reported an absorption spectrum of methanol in the region of 105–200 nm. A weak continuous feature in the 165–195 nm region shown in the bottom panel of Fig. 1 has been assigned to the S_1 ($3s \leftarrow n$) state. There are two sharp features, associated with the C–O stretching mode (spacing ~800 cm^{-1} in the 151–163 nm region and ~1000 cm^{-1} in the 140–151 nm region), were assigned to the component of the S_2 ($3p \leftarrow n$) state. Sominska *et al.*[9] reported the absorption spectra of CH_3OH, CH_3OD, and CD_3OD in a supersonic jet and assigned another vibrational mode (CH_3 rocking) for the system in the region of 151–163 nm. For wavelengths shorter than 140 nm, weak features were superimposed on a rising continuum, associated with transitions to higher Rydberg states.[8]

Photodissociation studies under molecular beam conditions provide crucial information on the mechanism of photodissociation processes.[11] In the studies of the infrared multiple photon dissociation of methanol,[12,13] OH + CH_3 initiated channel was observed on its ground state. In photolysis of methanol at 193 nm, however, the dominant process is O–H bond rupture *via* the S_1 state.[14] In the photolysis of CD_3OH at 193 nm, the ratio of H : D was determined to be 0.86 : 0.14; 82% of the total available energy was deposited into the translational degrees of freedom. Wen *et al.*[15] detected H and D atoms from the photodissociation of three isotopic variants of methanol using the high-*n*

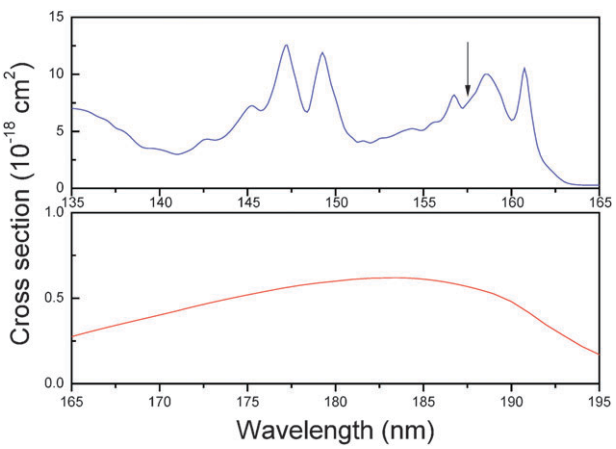

Fig. 1 The UV absorption spectrum of methanol, adapted from ref. 8. The lower panel shows the absorption spectrum in the 165–195 nm region. The broad continuum in this panel is attributed to the $3s \leftarrow n$ transition. The upper panel shows the absorption spectrum in the 135–165 nm region. The spectral features have been assigned to the $3p \leftarrow n$ transitions. The photolysis wavelength (157 nm) in this work is indicated by the arrow.

[a] *State Key Laboratory of Molecular Reaction Dynamics, Dalian Institute of Chemical Physics, Chinese Academy of Sciences, Dalian 116023, Liaoning, China. E-mail: xmyang@dicp.ac.cn; Fax: +86 411 84379876; Tel: +86 411 84379956*
[b] *Department of Molecular and Laser Physics, University of Nijmegen, 6525 ED Nijmegen, The Netherlands. E-mail: parker@science.ru.nl; Fax: +31 24 3653311; Tel: +31 24 3653423*
[c] *Institute of Theoretical Chemistry, University of Nijmegen, 6525 ED Nijmegen, The Netherlands*

 This journal is © the Owner Societies 2011

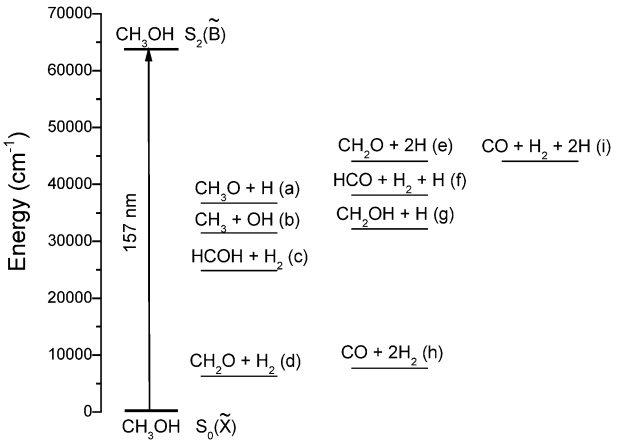

Fig. 2 Energy level diagram of methanol and energetically possible dissociation channels in this experiment. The available energy for a given channel is the difference in height between the photon energy and the channel enthalpy. See ref. 18 for more details.

Rydberg atom time-of-flight (HRTOF) technique.[16] Their results were in reasonable agreement with the previous result by Satyapal *et al.* (ref. 14) Photodissociation of methanol at 157 nm *via* the S_2 state is much more complicated. Fig. 2 shows an energy level diagram of methanol and at 157 nm a large number of dissociation channels are energetically possible. Harich *et al.*[17,18] measured photofragment translational spectra of three isotopic variants of methanol using the molecular beam photodissociation apparatus, and revealed three different atomic H loss processes and three molecular hydrogen elimination channels. More recently, Yuan *et al.*[19] studied the atomic hydrogen elimination channel using the H-atom Rydberg tagging technique. They observed vibrational structures for the $H + CH_3O$ channel. Lee *et al.*[20] studied methanol photodissociation using a TOF molecular beam mass spectrometer and found that the products angular distribution parameter β is negative, which revealed that the transition dipole moment was likely to be perpendicular to the C–O–H plane at 157 nm.

Theoretical studies[21–25] were also performed on the dynamics of methanol photodissociation. Dissociation energies of the O–H, C–H, and C–O bonds of methanol computed with a modified coupled-pair-functional method are in good agreement with the experimental values.[21] *Ab initio* calculations[22,23] were carried out for the three low-lying potential-energy surfaces (PES) of methanol. The S_0 (bound) PES correlates with $CH_2O + H_2$ (18.1 kcal mol^{-1})[24] which is the first energetically open dissociation channel. The S_1 PES has a large Rydberg character[22] in the region near the equilibrium bond length and is purely repulsive in the O–H coordinate, consistent with the continuous character of the first absorption band of methanol. In the C–O coordinate, there is a dissociation barrier of 0.58 eV, which prevents rupture of this bond on the S_1 PES at 193 nm.[15] Marston *et al.*[25] performed a wave packet calculation to investigate the function of the initial vibrational excitation on S_1. The relative branching ratio of CH_3O + H *versus* CH_3 + OH depends on both the initial vibrational excitation of methanol and the photon energy. The S_2 state is a bound state with an avoided crossing between S_2 ($3p \leftarrow n$) and S_1 ($3s \leftarrow n$) near the equilibrium geometry along the O–H and C–O bond coordinates.

For photolysis of methanol at 157 nm, the C–O bond cleavage channel was also observed.[18,20] Most recently, the 157 nm photoexcitation of solid methanol at 90 K was studied.[26] Using resonance-enhanced multiphoton ionization (REMPI) detection technique, the desorbed CH_3 ($v_2 = 0$) and OH ($v = 0,1$) radicals were observed near the solid surface. However, information on the correlation between the vibrational levels of the OH and CH_3 products has not been obtained thus far for CH_3OH photodissociation in the gas phase. Product pair correlation measurements were shown by Gericke,[27] Wodtke[28] and Liu[29] to carry insightful imprints of the concerted motions of atoms upon old bond rupture and new bond formation in chemical reactions. Similar insights into photodissociation processes can be expected, but in both cases a quantitative interpretation is contingent on the availability of accurate potential energy surfaces.

In this work, we present experimental results on the photodissociation of CH_3OH at 157 nm using the velocity map ion imaging method.[30] The CH_3 product was detected using (2 + 1) REMPI detection. In combination with velocity map ion imaging, this allows us to probe the CH_3 vibrational state specific dissociation dynamics as well as the state-to-state correlation between OH (v) and CH_3 (v_2) in the CH_3OH photodissociation at 157 nm.

2. Experimental methods

CH_3OH photodissociation at 157 nm was studied using velocity map ion imaging apparatus, which has been described previously.[31,32] A pulsed valve (Jordan) equipped with a 0.5 mm nozzle produced a ~100 μs pulsed molecular beam of CH_3OH seeded in He at 1 bar stagnation pressure. The mixture was prepared by feeding the carrier gas through liquid CH_3OH in a stainless steel bubbler, held at 0 °C to obtain a CH_3OH vapor pressure of ~30 Torr. The CH_3OH (99.9%) sample was purchased from Aldrich and the sample was used without further purification. At a distance of 20 mm downstream from the nozzle, the expanded beam passes through a skimmer with a 1 mm diameter aperture that separated the source and detection chambers. About 60 mm downstream from the nozzle the collimated beam passed through a 2 mm hole in a repeller electrode plate and propagated further along the axis of the 360 mm long time-of-flight tube of the ion imaging detector.

The CH_3OH molecular beam was intercepted by a 157 nm laser beam, which was generated by a commercial F_2 excimer laser (PSX-100) with 10 Hz repetition rate. In order to avoid multiphoton complications, only about 0.1 mJ pulse^{-1} of the 157 nm photolysis light was focused into the CH_3OH beam with a CaF_2 lens of 15 cm focal length. A commercial 157 nm thin film polarizer (Laseroptik GmbH) was used to produce linearly polarized 157 nm light. The resulting methyl radical fragments were photoionized about 20 ns later by a probe laser beam produced by doubling the output of a tunable dye laser (Radiant Narrowscan), which was pumped by the second harmonic of a Continuum Surelite Nd:YAG laser. The methyl radical ground state was probed on the strong Q branch

Published on 26 November 2010 on http://pubs.rsc.org | doi:10.1039/C0CP01794A
Downloaded by Radboud Universiteit Nijmegen on 06 November 2012

Published on 26 November 2010 on http://pubs.rsc.org | doi:10.1039/C0CP01794A
Downloaded by Radboud Universiteit Nijmegen on 06 November 2012

of the 0_0^0 band (the (2 + 1) REMPI transition goes through the $3p_z$ state). The higher lying umbrella modes (probed on the 2_1^1, 2_2^2, and 2_3^3 bands) were measured as well.[33,34] About 1 mJ of the probing laser was focused into the CH_3OH photolysis region using a lens of also 15 cm focal length. During image acquisition, the probe laser was fixed at the peak wavelengths (333.46 nm, 329.42 nm, 325.94 nm, and 322.70 nm) of the chosen REMPI transition.

The two laser beams were spatially overlapped in the CH_3OH beam at a middle position between the repeller and the extractor electrode. The electric field polarization direction of the pump laser was set to be perpendicular to the time-of-flight axis and that of the probe laser was set to be perpendicular or parallel to the axis. The images were collected by an imaging detector with dual 40 mm diameter multi-channel plates coupled to a phosphor screen. A cooled charge coupled device (CCD) camera was used to record the ion signals on the phosphor screen using the event counting program.[35]

3. Result and discussion

Fig. 3 displays the raw CH_3 (v_2 = 0) images (quadrant averaged) of CH_3OH photodissociation at 157 nm, obtained by accumulating the REMPI CH_3^+ signals over 50 000 laser shots with background subtraction. The background was taken using both lasers but without the molecular beam. The vertical arrow shows the polarization direction of the pump laser. The polarization direction of the probe laser was parallel with the arrow for Fig. 3A, while the probe laser polarization is perpendicular to the image plane for Fig. 3B. As can be seen, there were two main features of CH_3 signals: the outer rings and the inner structure. Well resolved anisotropic outer rings were measured in the images and these structures are easily assigned to the vibrational states of the partner OH product in the $OH + CH_3$ binary dissociation process. The distributions of outer rings were the same for the two polarization settings in the experiment, suggesting that the outer rings are due to the pump laser. For the inner part, significant differences between the images with the two polarization settings were observed. By comparing the images in Fig. 3, it is quite clear that the anisotropic distribution of the inner part was dependent on the polarization direction of the probe laser. It is well known that the REMPI detection process of CH_3 fragments is minimally sensitive to its alignment,[36], therefore the inner part of the observed CH_3^+ signal is clearly a probe laser induced process.

From the raw ion images, which are 3D images crushed to 2D, the reconstructed images could be obtained by Abel inversion. Fig. 4 shows the reconstructed 3D images, in which the polarization directions of the pump and the probe lasers were parallel to the arrow indicated. The reconstructed images were obtained using the Basex program.[37] The outer rings that correspond to the OH partner product in different vibrational states for the CH_3 product at v_2 = 0, 1, 2, and 3 in the umbrella vibration mode were very well resolved. As can be seen directly in the images, the outer ring structures of the OH vibrational excited products corresponding to different CH_3 umbrella mode excited states are obviously different, indicating a clear vibrational state-to-state correlation between the OH and CH_3 products.

Total kinetic energy distributions in the center-of-mass frame for the different CH_3 (v_2) products were extracted from Fig. 4. The results were shown for the four individual umbrella mode vibrational states of CH_3 in Fig. 5. The OH vibrational distributions are inverted and peak at v = 4 for the CH_3 ground state and at v = 3 for all the vibrationally excited states. From Fig. 5, the vibrational excitation of OH (v) clearly decreases as the CH_3 umbrella mode excitation increases. The average product kinetic energy, (E_{trans}), indicates that about 65% of the total available energy[38,39] is partitioned into the translational degree of freedom for the different CH_3 (v_2 = 0, 1, 2, and 3) product channels. This implies that C–O bond cleavage of CH_3OH at 157 nm excitation is a fast dissociation process. These results are consistent with previous experiments.[18,20]

To extract the correlated vibrational distribution of the OH product, a qualitative simulation of the energy distribution was carried out. Each rotational peak was simulated in energy

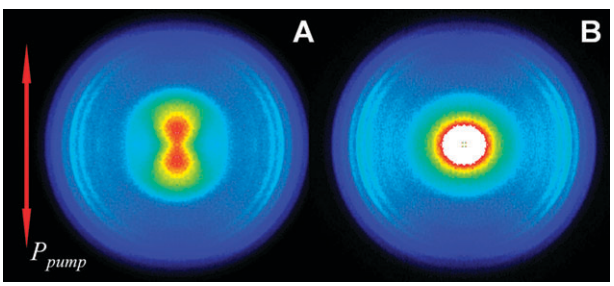

Fig. 3 Raw CH_3 images of the CH_3 (v_2 = 0) products from the photodissociation of CH_3OH at 157 nm are probed *via* the Q branch of the $3p_z$ ($^2A_2'' \leftarrow X^2A_2''$) 2 + 1 REMPI transition: (A) The polarization of the probe laser is parallel to the photolysis laser; (B) The polarization of the probe is perpendicular to the photolysis laser, and to the paper plane. The double arrow indicates the polarization of the photolysis laser.

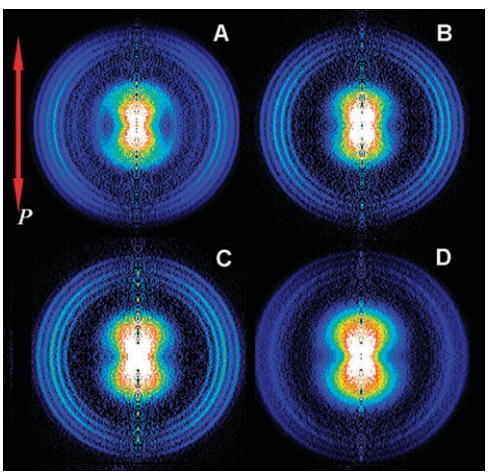

Fig. 4 Inverted images of CH_3 (v_2 = 0) (A), CH_3 (v_2 = 1) (B), CH_3 (v_2 = 2) (C) and CH_3 (v_2 = 3) (D) products from the photodissociation of methanol at 157 nm. The double arrow indicates the polarization both of the pump and probe lasers. The ring features correspond to the vibrational states of the coincident OH (v) product.

 This journal is © the Owner Societies 2011

Published on 26 November 2010 on http://pubs.rsc.org | doi:10.1039/C0CP01794A
Downloaded by Radboud Universiteit Nijmegen on 06 November 2012

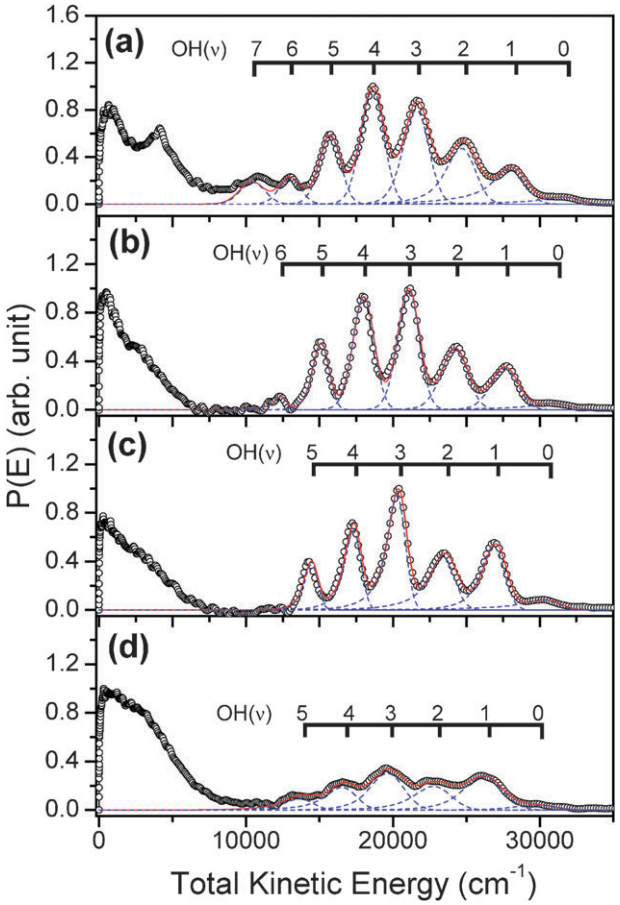

Fig. 5 The product total kinetic energy distributions (black empty circles) derived from the inverted velocity images in Fig. 4 for the OH (v) + CH_3 (v_2) channels. The red lines are the fitting results and the blue dash lines are the individual OH vibrational components.

space using a Gaussian line shape of fixed energy width (800 cm^{-1}) that reflected our instrumental contribution. Within one vibrational peak, the OH rotational state distribution was assumed to be a Boltzmann distribution. The rotational temperature and the intensity were varied to fit each vibrational peak. The simulated results were also shown in Fig. 5. The fitting error was estimated to be about 10%, which is also reflected in the varying (rotational) widths of the vibrational peaks. Spin-orbit and lambda doublet splitting were not considered in the fitting.

The results of the such simulation reveals that the rotational excitation is about ~1500 K in the OH (v) + CH_3 (v_2) channel, which is considerably lower than the vibrational excitation of the OH product. OH rotational distributions for all the CH_3 umbrella mode vibrational states are similar, suggesting that the four channels have similar transition states in the dissociation.

Angular distributions of the OH (v) + CH_3 (v_2) channel were also obtained for the four CH_3 internal states by integrating the imaging signals over the outer radius region. The overall anisotropy parameters were determined by fitting the angular distributions and the values were −0.53, −0.70, −0.60, and −0.49 for the different internal methyl radical states (v_2 = 0–3), respectively. The large negative anisotropy parameters again suggest that the OH + CH_3 (v_2 = 0–3) dissociation channel is a fast dissociation process following a perpendicular electronic excitation. Our results are higher than those of previous experiments (β = −0.75)[20] which measured the overall anisotropy parameters of all of the internal states of the CH_3 product. The β value of CH_3 (v_2 = 0) is higher than that of the first umbrella mode excited state of the CH_3 fragment, indicating that the H–O–C angle of the transition state forming CH_3 (v_2 = 1) is likely to be a little smaller than that forming CH_3 (v_2 = 0). With further increase in excitation, less anisotropic results were observed. However, there is no significant difference for the geometry of their transition states.

From the simulations, the correlated OH vibrational distributions for the four CH_3 production states were obtained (Fig. 6A). As the excitation of the CH_3 umbrella mode increases, the peak of the correlated OH vibrational state distribution shifts to lower vibrational states. The maximum OH vibrational excitation also decreases as the correlated CH_3 product umbrella vibration excitation increase. This shows clearly that the vibrational excitation of the correlated OH product is anti-correlated to the CH_3 umbrella vibration excitation. The correlated OH vibrational distributions are, however, not very smooth distributions. One can clearly see that the OH (v = 2) vibrational state population is noticeably smaller than the neighboring OH vibrational states. Anisotropy parameters for the individual OH vibrational state products that correspond to the four CH_3 states were also obtained (Fig. 6B). The anisotropy parameters are generally lower for OH products with less vibrational excitation. It means that the H–C–O angle of the transition state increases slightly with the internal energy of OH increasing. However, no dramatic changes to the anisotropy parameters were found.

In all the images, the inner part signals are both photolysis laser (157 nm) and probe laser dependent. This means that the detected CH_3 product comes from both the photolysis laser and probe laser. In the middle part of the inner region an

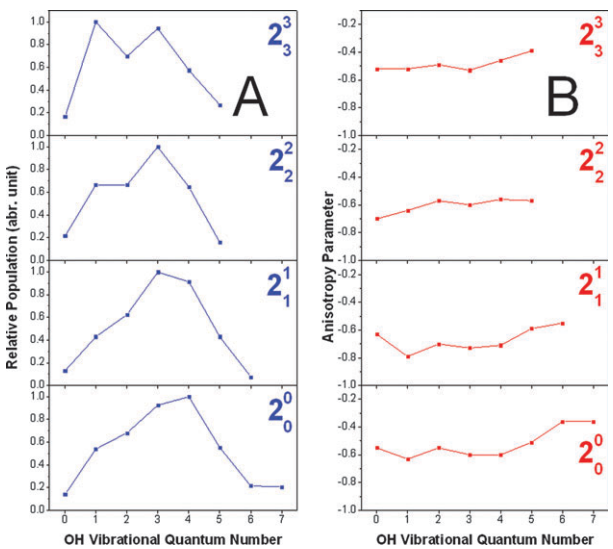

Fig. 6 (A) Relative vibrational state distribution of the OH co-products for different umbrella states of the CH_3 (v_2) product; (B) Anisotropy parameter for individual OH vibrational states correlated to the four CH_3 (v_2) states.

Published on 26 November 2010 on http://pubs.rsc.org | doi:10.1039/C0CP01794A
Downloaded by Radboud Universiteit Nijmegen on 06 November 2012

anisotropic *p*-orbital shape appears, which is a shape usually characteristic of dissociative ionization, $CH_3OH \rightarrow CH_3^+ + OH + e^-$. This is superimposed over what we suggest is a CH_3 (v_2) product with an overall β parameter of about 0.65. This part of image for different CH_3 (v_2) products is slightly different. From the images, it is obvious that the CH_3 products have much smaller kinetic energies than those from the OH + CH_3 product channel. The origin of these slow CH_3 products is quite intriguing. First of all, these slower CH_3 products were not produced from 157 nm alone, they are the products of both photolysis laser and probe laser. Since the probe laser at 333.5 nm is unlikely to generate any CH_3 containing species from CH_3OH, 157 nm photolysis of CH_3OH is the only likely source of CH_3 containing species. It is known that 157 nm photolysis of methanol can also produce the CH_3O + H product channel, and the excited CH_3O species generated could also be dissociated in the wavelength region of the probe laser, yielding $CH_3(X^2A_1, v = 0) + O(^3P)$.[40–42] Such a two-step dissociation process can certainly produce slower CH_3 products, and with angular anisotropy. The slower CH_3^+ products could also be generated from the photodissociation of CH_3O^+, which is produced from the multiphoton ionization of CH_3OH by the 157 nm laser.[43] However, the contribution of this possible process to the slower CH_3 signals, and the ratio of signal strength for CH_3 arising from CH_3O *versus* CH_3OH cannot be evaluated quantitatively.

Returning to the main $CH_3OH \rightarrow CH_3 + OH$ signal, *ab initio* calculations[22,23,25] show that there is an avoided crossing between the 3*s* and the 157 nm photoexcited 3*p* surfaces, suggesting that there is strong coupling between the two surfaces. Because both the C–O bond and the O–H bond are repulsive on the 3*s* surface, it seems clear that once the system undergoes fast internal conversion to the 3*s* surface, C–O bond breaking will be accompanied by high vibrational excitation of the OH product. The optical signature of excitation to the 3*p* surface shows that significant vibrational excitation of the CH_3OH parent molecule takes place, which should be reflected in the vibrational excitation of the CH_3 product. The correlated OH vibrational distributions measured here for state selected CH_3 (v_2) products should thus provide a sensitive test for the accuracy of the multidimensional potential energy surfaces describing methanol photodissociation.

4. Conclusions

The OH + CH_3 channel in the photodissociation of CH_3OH at 157 nm was investigated using velocity map imaging of the CH_3 fragments. The main structures of the outer ring signals are assigned to the binary OH + CH_3 dissociation channel. The correlated OH vibrational state distributions for the CH_3 (v_2 = 0, 1, 2, and 3) products were measured. Large anisotropy parameters were measured for the OH + CH_3 channel, consistent with a fast dissociation process. The inverted OH vibrational distributions are obtained as a consequence of the force acting in the crossing from the bound S_2 excited state to the unbound S_1 excited state. The OH vibrational state distributions are not very smooth with a dip for the OH (v = 2) population. Wavefunctions on the ground and excited states will contain nodal patterns that could show better or worse overlap for different vibrational states, which means that the Franck–Condon overlap could alternate for subsequent vibrational wavefunctions, leading to the behavior observed in the experiment. The results also show that a significant amount of the total available energy was deposited into the translational energy and that the product rotational temperature of the OH product is about 1500 K. In addition to the OH + CH_3 binary dissociation channel, slower CH_3 products were also observed and were attributed to a two-step photodissociation process.

Acknowledgements

Z. Chen gratefully acknowledges Konstantin Vidma for his experimental support. This work was supported by the Nederlandse Organisatie voor Wetenschappelijk Onderzoek, and partially by the National Science Foundation of China, the Ministry of Science and Technology and the Chinese Academy of Sciences.

References

1 E. Murad, W. Swider, R. A. Moss and S. Toby, *Geophys. Res. Lett.*, 1984, **11**, 147–150.
2 J. M. Greenberg, *Astron. Astrophys.*, 1998, **330**, 375.
3 J. Davies and T. Kerr, *Int. Astron. Union Circ.*, No. 7201, 1 1999.
4 Y. L. Yung and W. B. DeMore, *Photochemistry of Planetary Atmospheres*, Oxford University Press, New York, 1999, pp. 99–101.
5 T. Jacq, C. M. Walmsley, R. Mauersberger, T. Anderson, E. Herbst and F. C. de Lucia, *Astron. Astrophys.*, 1993, **271**, 276.
6 M. B. Robin, *Higher Excited States of Polyatomic Molecules*, Academic, Orlando, FL, 1985, p. 245, and references therein.
7 J. G. Galvert and J. N. Pitts, *Photochemistry*, Wiley, New York, 1966, p. 441.
8 J. B. Nee, M. Suto and L. C. Lee, *Chem. Phys.*, 1985, **98**, 147–155.
9 E. Sominska and A. Gedanken, *J. Mol. Spectrosc.*, 1996, **175**, 234–238.
10 B. Cheng, M. Bahou, W. Chen, C. Yui and Y. Lee, *J. Chem. Phys.*, 2002, **117**, 1633–1640.
11 R. Schinke, *Photodissociation Dynamics*, Cambridge University Press, Cambridge, 1993.
12 S. E. Bialkowski and W. A. Guillory, *J. Chem. Phys.*, 1977, **67**, 2061–2067.
13 R. Schmiedl, U. Meier and K. H. Welge, *Chem. Phys. Lett.*, 1981, **80**, 495–498.
14 S. Satyapal, J. Park, R. Bersohn and B. Katz, *J. Chem. Phys.*, 1989, **91**, 6873–6879.
15 Y. Wen, J. Segall, M. Dulligan and C. Wittig, *J. Chem. Phys.*, 1994, **101**, 5665–5671.
16 M. N. R. Ashfold, D. H. Mordaunt and S. H. S. Wilson, *Adv. Photochem.*, 1996, 217.
17 S. Harich, J. J. Lin, Y. T. Lee and X. Yang, *J. Chem. Phys.*, 1999, **111**, 5–9.
18 S. Harich, J. J. Lin, Y. T. Lee and X. Yang, *J. Phys. Chem. A*, 1999, **103**, 10324–10332.
19 K. Yuan, Y. Cheng, F. Wang and X. Yang, *Chin. J. Chem. Phys.*, 2008, **21**, 301–307.
20 S. H. Lee, H. I. Lee and Y. T. Lee, *J. Chem. Phys.*, 2004, **121**, 11053–11059.
21 C. W. Bauschlicher, Jr., S. R. Langhoff and S. P. Walch, *J. Chem. Phys.*, 1992, **96**, 450–454.
22 E. Kassab, J. T. Gleghorn and E. M. Evleth, *J. Am. Chem. Soc.*, 1983, **105**, 1746–1753.
23 R. J. Buenker, G. Olbrich, H. P. Schuchmann, B. L. Schurmann and C. Sonntag, *J. Am. Chem. Soc.*, 1984, **106**, 4362–4368.
24 S. P. Walch, *J. Chem. Phys.*, 1993, **98**, 3163–3167.

 This journal is © the Owner Societies 2011

View Online

25 C. C. Marston, K. Weide, R. Schinke and H. U. Suter, *J. Chem. Phys.*, 1993, **98**, 4718–4727.
26 T. Hama, M. Yokoyama, A. Yabushita, M. Kawasaki, P. Wickramasinghe, W. Guo, H. P. Loock, M. N. R. Ashfold and C. M. Western, *J. Chem. Phys.*, 2009, **131**, 224512.
27 K.-H. Gericke, *Phys. Rev. Lett.*, 1988, **60**, 561–564.
28 C. G. Morgan, M. Drabbels and A. M. Wodtke, *J. Chem. Phys.*, 1996, **105**, 4550–4555.
29 K. Liu, *Phys. Chem. Chem. Phys.*, 2007, **9**, 17–30.
30 A. T. J. B. Eppink and D. H. Parker, *Rev. Sci. Instrum.*, 1997, **68**, 3477–3484.
31 S. M. Wu, X. M. Yang and D. H. Parker, *Mol. Phys.*, 2005, **103**, 1797–1807.
32 Z. Chen, F. Liu, B. Jiang, X. Yang and D. H. Parker, *J. Phys. Chem. Lett.*, 2010, **1**, 1861–1865.
33 A. T. J. B. Eppink and D. H. Parker, *J. Chem. Phys.*, 1999, **110**, 832–844.
34 R. Schott, J. Schlutter, M. Olzmann and K. Kleinermanns, *J. Chem. Phys.*, 1995, **102**, 8371–8377.
35 L. Dinu, A. T. J. B. Eppink, F. Rosca-Pruna, H. L. Offerhaus, W. J. van der Zande and M. J. J. Vrakking, *Rev. Sci. Instrum.*, 2002, **73**, 4206–4213.
36 M. H. M. Janssen, D. H. Parker, G. O. Sitz, S. Stolte and D. W. Chandler, *J. Phys. Chem.*, 1991, **95**, 8007–8013.
37 V. Dribinski, A. Ossadtchi, V. A. Mandelshtam and H. Reisler, *Rev. Sci. Instrum.*, 2002, **73**, 2634–2642.
38 A. Stolow and Y. T. Lee, *J. Chem. Phys.*, 1993, **98**, 2066–2076.
39 D. D Wagman, W. H. Evans, W. B. Parker, S. H. Schumm, I. Halow, S. M. Bailey, K. L. Churney and R. L. Nutall, *J. Phys. Chem. Ref. Data*, 1982, **11**(Suppl. 1).
40 D. E. Powers, M. B. Pushkarsky and T. A. Miller, *J. Chem. Phys.*, 1997, **106**, 6863–6877.
41 D. E. Powers, M. B. Pushkarsky and T. A. Miller, *J. Chem. Phys.*, 1997, **106**, 6878–6884.
42 D. L. Osborn, D. J. Leahy and D. M. Neumark, *J. Phys. Chem. A*, 1997, **101**, 6583–6592.
43 J. G. Philis, *Chem. Phys. Lett.*, 2007, **449**, 291–295.

Published on 26 November 2010 on http://pubs.rsc.org | doi:10.1039/C0CP01794A
Downloaded by Radboud Universiteit Nijmegen on 06 November 2012